Cost-Effective Implementation of Filters in Millimeter Wave Range on Printed Circuit Boards

Florian Keck[#1], Franz Xaver Röhrl[~2], Stefan Zorn[~3]
[#]DIT Deggendorf Institute of Technology, Dieter-Görlitz-Platz 1, 94469 Deggendorf, Germany
[~]Rohde & Schwarz GmbH & Co. KG, Werk Teisnach, Kaikenrieder Straße 27, 94244 Teisnach, Germany
{[1]florian.keck}@stud.th-deg.de, {[2]franz.roehrl, [3]stefan.zorn}@rohde-schwarz.com

***Abstract*—The fabrication of filters in millimeter wave range with conventional printed circuit technology is subjected to some disadvantages like (high insertion loss, shielding and small dimensions) compared to air-filled waveguides. The here presented submount technology covers a frequency range from 33 GHz to 110 GHz with a very low insertion loss of roughly 1 dB within a length of 22 mm. Passive structures like filters can be implemented in such submounts. Therefore, a ninth order Chebyshev band-pass filter in a WR19 submount waveguide is realized in the U-band. The design is split into two steps, an analytic concept and an optimization. The filter has a simulated bandwidth of 10.4 GHz with a center frequency of 49.2 GHz. It features a low pass-band insertion loss of 0.67 dB and high stop band insertion loss in the lower and higher band, respectively 110 dB and 30 dB. The return loss in the pass-band is 20 dB.**

Keywords — band-pass filter, low loss transmission lines, air filled waveguide, submount, iris filter, millimeter wave, Chebyshev, U-band, WR19, WR15, WR12, WR10

I. Introduction

The requirements for high-frequency systems in the millimeter wave range have risen massively in recent years. The main issues are high data rates and continuously increasing integration density. Besides the steady progressing miniaturization in electronics industry, low fabrication costs and high quality are required simultaneously. Low-loss transmission lines are a key technology for millimeter wave applications. In [1], a GCPW (grounded coplanar waveguide) with reduced attenuation by partially removed substrate was analyzed. The measurement showed an improved attenuation of 0.25 dB/cm at 90 GHz. Another technology of great interest for many practical applications in standard low cost printed circuit board (PCB) manufacturing processes is the substrate integrated waveguide (SIW), because of its robustness against production tolerance [2]. With regard to quality factor and losses, these devices are a good compromise between the performance of planar circuits and classical waveguides. Conventional rectangular waveguides are often preferred for low-loss applications. They show negligible losses, since the electric field is lead in air (dielectric constant $DK_{air} \approx 1$ and dissipation factor $DF_{air} \approx 0$).

Therefore, high research effort is taken to implement waveguides on PCBs to combine the benefits of the SIW and the classical rectangular waveguide. Devices like the air filled substrate integrated waveguide (AFSIW) already showed, that passive structures (e.g. waveguides or filters) produced in AFSIW technology have a better RF performance than the conventional SIW ([3]-[4]). In [3] and [4] the AFSIW was realized as planar structure, analyzed and compared to conventional SIW up to 60 GHz. Whereas in this paper, the air filled waveguides are realized from 33 GHz to 110 GHz with the EIA standard (WR22 to WR10). A great advantage of using waveguides as submounts is the fact that the necessary manufacturing techniques are available in conventional circuit board technology. In addition, the submounts can be fully assembled in SMD production lines due to their smooth surface.

II. Manufacturing of Submount Waveguides

Producing a waveguide as a submount allows the use of cost effective substrates (e.g. FR-4) as they also can be used for the production of the baseboard. For this purpose, a cavity depth milling technology is used to create the waveguide structures. Subsequently, the structures are coated with copper ($25\,\mu\mathrm{m}$) and silver ($250\,\mathrm{nm}$), to create a conductive surface. The produced WR10 waveguide submounts are shown in Fig.1.

Fig. 1. Manufactured 22 mm and 44 mm long WR10 waveguide submounts

III. Overview of Possible Waveguides

The submount technology is limited by its transition from GCPW to waveguide and the height of the waveguide channel. The lower boundary is defined by the maximum compressible thickness of a layer stackup, which is $3.6\,\mathrm{mm}$. The upper boundary is set by the line width of the transition (min. $125\,\mu\mathrm{m}$). According to EIA standard the ascertainable frequency band ranges from 33 GHz to 110 GHz. Due to the

skin depth δ_s, the return loss α increases proportional with frequency f (see equation (1)).

$$\alpha = \frac{1}{\delta_s} \; with \; \delta_s = \sqrt{\frac{1}{\pi f \sigma \mu}} \qquad [6] \qquad (1)$$

TABLE I displays simulated waveguides with a channel length of 22 mm.

TABLE I
OVERVIEW OF SIMULATED WAVEGUIDES WITH A LENGTH OF 22 MM

EIA Size	Frequency band	Return loss	Insertion loss
WR19	U-band	19.6 dB	0.7 dB
WR15	V-band	20.0 dB	0.8 dB
WR12	E-band	19.1 dB	0.9 dB
WR10	W-band	17.1 dB	1.2 dB

IV. DESIGN IRIS WAVEGUIDE FILTER

To demonstrate the capabilities of the submount waveguide technology a high-slope waveguide band-pass filter is realized in the U-band. The pass-band covers the range from 44 GHz to 54 GHz with a high stop-band attenuation. The resonator structure is based on iris-cavities as presented in [5].
Firstly, the required filter order is determined by a low-pass filter prototype. To achieve sharp stop-band attenuation, a Chebyshev filter characteristic is chosen. For transforming it into a band-pass response, a frequency substitution is used:

$$\omega' \leftarrow \frac{1}{\delta} \cdot \left(\frac{\omega_r}{\omega_0} - \frac{\omega_0}{\omega_r} \right) \qquad [6] \qquad (2)$$

where δ is the fractional bandwidth of the pass-band, ω_0 the center frequency and ω_r the rejected frequency. For a return loss of 20 dB the equivalent ripple deviation L_{as} is 0.0432 dB (see equation (3)).

$$ReturnLoss_{dB} = 10 \cdot log \left(10^{\frac{L_{as_{dB}}}{10}} - 1 \right) \qquad [7] \qquad (3)$$

Then, the filter order is determined using equation (4).

$$N \geq \frac{arccosh \left(\sqrt{\frac{10^{\frac{L_{as}}{10}} - 1}{10^{\frac{L_{ar}}{10}} - 1}} \right)}{arccosh\left(\omega'\right)} \qquad [6] \qquad (4)$$

With a fractional bandwidth δ of 2.04, a center frequency f_c of 49 GHz and a necessary rejection level L_{ar} of 50 dB at $f_r = 58$ GHz, a filter order of $N = 9$ meets the requirements. Furthermore the chosen filter order should be odd to achieve matching in- and outputs. Fig. 2 shows the estimated band-pass filter with its pass- and stop-bands (transparent blue areas).
Secondly, the synthesis continues with the low-pass filter prototype normalized in terms of frequency and impedance. Then suitable transformations are applied to convert the low-pass filter to the desired operating frequency and impedance level. Afterwards, the coupling coefficients are translated into physical dimensions. Finally, the physical dimensions of the design is optimized with CST Microwave Studio®. The filter transformation is done by a Matlab® script.

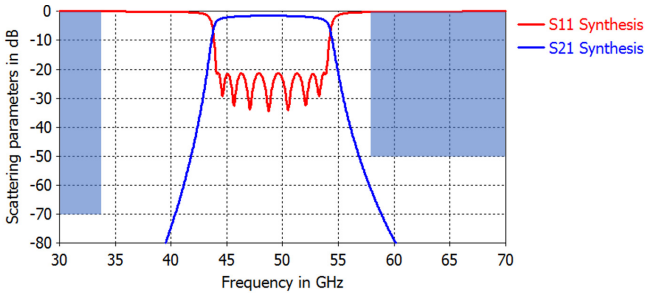

Fig. 2. Estimated band-pass filter from CST Filter Designer 3D®

A. Equal-Ripple Low-Pass Filter Element Values

For the base low-pass prototype, the Chebyshev coefficients g_i are necessary. They are determined with equation (5) to (9).

$$\beta = ln \left[coth \left(\frac{|L_{as}|}{17.37} \right) \right] \qquad \gamma = sinh \left(\frac{\beta}{2N} \right) \qquad [6] \quad (5)$$

$$a_i|_{i=1\ldots N} = sin \left(\frac{(2i-1)\,\pi}{2N} \right) \qquad [6] \qquad (6)$$

$$b_i|_{i=1\ldots N} = \gamma^2 + sin^2 \left(\frac{i\pi}{N} \right) [6] \qquad (7)$$

$$g_0 = 1 \qquad g_1 = \frac{2a_1}{\gamma} \qquad g_i|_{i=2\ldots N} = \frac{4a_i a_{i-1}}{b_{i-1} g_{i-1}} \qquad [6] \quad (8)$$

$$g_{N+1} = 1 \; for \; N \; odd$$
$$g_{N+1} = coth^2 \left(\frac{\beta}{4} \right) \; for \; N \; even \qquad [6] \qquad (9)$$

These are determined to: $g_0 = g_{10} = 1$, $g_1 = g_9 = 1.0234$, $g_2 = g_8 = 1.4619$, $g_3 = g_7 = 1.9837$, $g_4 = g_6 = 1.6778$, $g_5 = 2.0648$.

B. Synthesis

The filter consists of nine cavity resonators placed in a row which are each l_i long and being coupled by irises of opening width b_i (see Fig. 3).

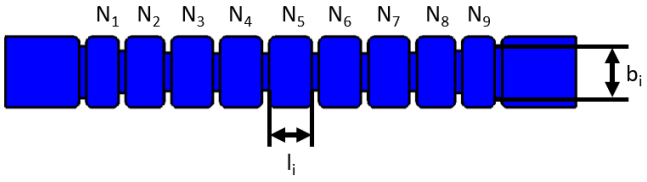

Fig. 3. Top view of the ninth order iris band-pass filter

The irises can be modeled by a shunt susceptance B_i. The design equations for that are derived by Collin [8] and presented here below for a Chebyshev characteristic:

$$\overline{B}_1 = \frac{1 - \frac{\omega}{g_1}}{\sqrt{\frac{\omega}{g_1}}} \qquad [8] \qquad (10)$$

$$\overline{B}_2 = \frac{1}{\omega} \left(1 - \frac{\omega^2}{g_1 g_2} \right) \sqrt{g_1 g_2} \qquad [8] \qquad (11)$$

$$\overline{B}_i|_{i=3\ldots N-1} = \frac{1}{\omega}\left(1 - \frac{\omega^2}{g_i g_{i-1}}\right)\sqrt{g_i g_{i-1}} \qquad [8] \qquad (12)$$

$$\overline{B}_N = \frac{1 - \frac{\omega R}{g_N}}{\sqrt{\frac{\omega R}{g_N}}} \; with \; R = 2k^2 + 1 - 2k\sqrt{1+k^2}$$
$$k = 10^{\frac{L_{ar_{dB}}}{10}} - 1 \qquad [8] \qquad (13)$$

with g_k are the low-pass prototype Chebyshev coefficients and ω is $\frac{\pi}{2}\frac{\beta_2 - \beta_1}{\beta_0}$. The phase constant of an air filled waveguide is given in equation (14), where c_0 is the speed of light and a is the width of the waveguide.

$$\beta_n = \sqrt{\left(\frac{2\pi f_n}{c_0}\right) - \left(\frac{\pi}{a}\right)^2} \qquad [8] \qquad (14)$$

The center of the band occurs at $\beta_0 = \sqrt{\beta_1 \beta_2}$. The physical length of each cavity l_i is given by:

$$l_i = \frac{\lambda_{g0}}{2} - \frac{\lambda_{g0}}{4\pi}\left(arctan\left(\frac{2}{\overline{B}_{k+1}}\right) + arctan\left(\frac{2}{\overline{B}_k}\right)\right)$$
$$with \; \lambda_{g0} = \frac{2\pi}{\beta_0} \qquad [8] \qquad (15)$$

To extract the width b_i of each iris later, the internal coupling coefficient $c_{i,i+1}$ from two adjacent cavities is calculated following:

$$c_{i,i+1} = \frac{BW}{f_0\sqrt{g_i g_{i+1}}} \qquad [9] \qquad (16)$$

Table II displays all determined data.

TABLE II
RESULTS OF THE ABOVE EQUATIONS FOR SUSCEPTANCE B_i, COUPLING COEFFICIENTS $k_{i,i+1}$, IRIS WIDTH b_i AND PHYSICAL CAVITY LENGTH l_i

Iris	1	2	3	4	5	6	7
$\overline{B}$ in S	0.679	1.765	2.761	3.002	3.075	3.075	3.002
c in %	20.28	16.77	12.05	11.25	11.02	11.02	11.25
b_i in mm	3.63	3.24	2.76	2.68	2.65	2.65	2.68

Cavity	1	2	3	4	5	6	7
l_i in mm	2.682	3.076	3.242	3.275	3.282	3.275	3.242

Iris	8	9	10
$\overline{B}$ in S	2.761	1.765	0.648
c in %	12.05	16.77	20.28
b_i in mm	2.76	3.24	3.63

Cavity	8	9
l_i in mm	3.076	2.673

C. Extraction of iris width

The coupling coefficients are extracted using the post processing function 3D Eigenmode Coupling Coefficient in CST Microwave Studio®. It uses equation (17) to calculate the coupling coefficient between mode number 1 (mode with lowest eigenfrequency) and mode number 2 (mode with second lowest eigenfrequency) [10].

$$\alpha = 2 \cdot \left|\frac{f_1 - f_2}{f_1 + f_2}\right| \qquad [10] \qquad (17)$$
$$with \; f_1 = fres(Mode\ 1) \; and \; f_2 = fres(Mode\ 2)$$

The setup for the investigation consists of two waveguide sections according to WR19 standard and is illustrated in Fig. 4. Both parts are separated by a movable and vertical iris.

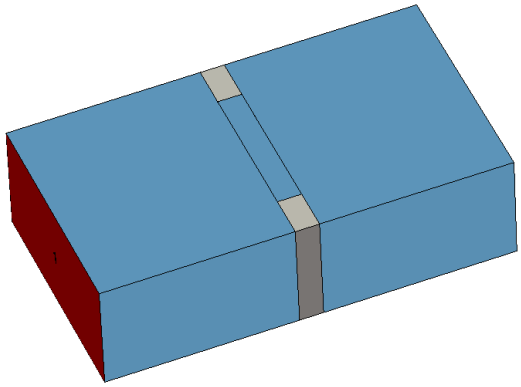

Fig. 4. Extraction model for the coupling coefficient

The iris has a width of $0.5\,\mathrm{mm}$ and is identical to the irises in the final model. The length of both sections must correspond to the waveguide wavelength at the center frequency λ_{g0}. The values presented in Table II are extracted from Fig. 5 and were used as initial values for optimization.

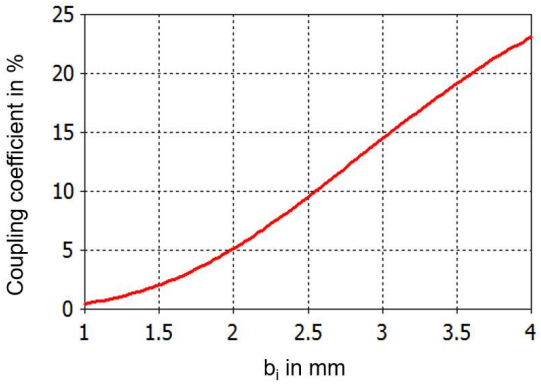

Fig. 5. Coupling coefficient as a function of the iris opening b_i

V. SIMULATION RESULT

The analytically filter design with the values from Table II is simulated and displayed in Fig. 6. The bandwidth of the filter with 9.8 GHz meets the requirements. Due to the fact, that the calculation assumes infinitesimal iris walls, the operating frequency band of the filter is shifted to lower

frequencies. A return loss of 6.2 dB is the consequence. An optimization decreases the cavity lengths to push the pass-band to its requested center frequency. Also each iris width is optimized to enhance the coupling between the resonators. The interaction of both improvements significantly improves the overall performance of the filter.

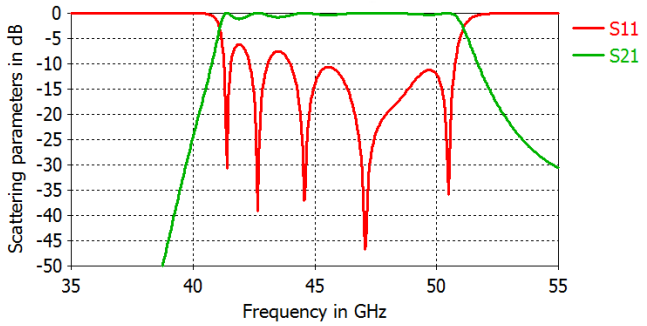

Fig. 6. Simulation result of the analytical filter design

The resulting scattering parameters are present in Fig. 7. The return loss of the resulting waveguide iris filter is better than 20 dB in the whole pass-band (44-54.4 GHz). This is given by a center frequency of 49.2 GHz and a bandwidth of 10.4 GHz.

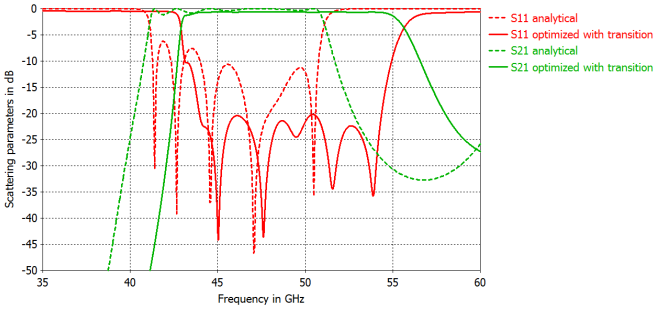

Fig. 7. Comparison between the analytic and optimized filter design

In terms of insertion loss, the simulation indicates a maximum value of 0.67 dB. Due to the fact, that only the roughness of the PCB is taken into account in the simulation, the insertion loss will be slightly higher. Through preceded measurements in [11], we assume a surface roughness R_q of $1\,\mu\mathrm{m}$. Therefore, the insertion loss is within the range of 1 dB. In the lower stop-band the filter has an attenuation of more than 110 dB. At the upper stop-band the attenuation is only around 30 dB. This is caused by the resonating structure, as the cavities are not only responsive for the desired TE_{101}-Mode for a width a of $4.78\,\mathrm{mm}$ at the center frequency, they are also sensitive for the TE_{101}-Mode for a width a of around $2.5\,\mathrm{mm}$ at 71 GHz. The second value for a derives from the smallest iris width b_i. Another simple verification method is the equation (18). With the values from above the resonating frequencies and the declaration is confirmed ($d = 3.87$ mm).

$$\begin{aligned} f_{mnl} &= c_0\sqrt{\left(\frac{m}{2a}\right)^2+\left(\frac{n}{2b}\right)^2+\left(\frac{l}{2d}\right)^2} \qquad [8] \\ \rightarrow\ f_{101} &= 49.9\ \mathrm{GHz}\,(a = 4.78\,\mathrm{mm}) \\ \rightarrow\ f_{101} &= 71.4\ \mathrm{GHz}\,(a = 2.5\,\mathrm{mm}) \end{aligned} \tag{18}$$

To improve the upper stop-band attenuation, a low-pass filter after the band-pass as in [2] would be fine. The whole filter with the GCPW to waveguide transition shows Fig. 8.

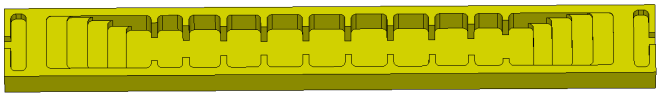

Fig. 8. Waveguide iris band-pass filter as submount with transition

VI. Conclusion

This paper presents a low cost air-filled waveguide iris band-pass filter in the U-band. The submount technology allows to combine the advantages of the waveguide technology with the low cost standard PCB technology in a new way. The analytically filter design in combination with one optimization step is an efficient process to receive such a band-pass filter. The simulation shows a high performance filter with a low insertion loss in the pass-band. Through the use of low-cost materials it is suitable for commercial applications.

Acknowledgment

The Project PaGAnIni is financially supported by the Bavarian Ministry of Economic Affairs, Regional Development and Energy. All kinds of support are gratefully acknowledged. The author also like to thank Rohde & Schwarz Teisnach for all the fabrication and measurement support.

References

[1] F. Sepaintner, A. Scharl, F. X. Röhrl, W. Bogner, and S. Zorn, "Simulation and Manufacturing of Low Loss PCB Structures with Additional Electromagnetic Field in Air," in *Proc. IEEE MTT-S International Microwave Workshop Series on Advanced Materials and Processes for RF and THz Applications (IMWS-AMP)*, Jul. 2019, pp. 94–96.

[2] F. X. Röhrl, R. Sammer, J. Jakob, W. Bogner, R. Weigel, U. Hassel, and S. Zorn, "Cost-effective SIW band-pass filters for millimeter wave applications a method to combine low tolerances and low prices on standard pcb substrates," in *Proc. 2017 47th European Microwave Conference (EuMC)*, Nuremberg, Germany, Oct. 2017, pp. 416–419.

[3] A. Ghiotto, F. Parment, T. Martin, T. Vuong, and K. Wu, "Air-filled substrate integrated waveguide — A flexible and low loss technological platform," in *Proc. 2017 13th International Conference on Advanced Technologies, Systems and Services in Telecommunications (TELSIKS)*, Nis, Serbia, Oct. 2017, pp. 147–149.

[4] F. Parment, A. Ghiotto, T. Vuong, J. Duchamp, and K. Wu, "Air-filled siw transmission line and phase shifter for high-performance and low-cost u-band integrated circuits and systems," in *Global Symposium on Millimeter-Waves (GSMM)*, 2015, pp. 1–3.

[5] Y. Zhai, Q. Wang, Z. Wang, and X. x. Gao, "The design of an iris waveguide filter at 35.75 ghz," in *2008 Global Symposium on Millimeter Waves*, 2008, pp. 348–350.

[6] D. M. Pozar, *Electromagnetic Waves and Antennas*. Hoboken ,New Jersey, USA: John Wiley & Sons, Inc., 2012.

[7] *CST STUDIO SUITE®Help*, 2020, section: Equiripple.
[8] R. E. Collin, *Foundations for Microwave Engineering*. Hoboken ,New Jersey, USA: John Wiley & Sons, Inc., 1966.
[9] L. Harle, Ph.D. dissertation.
[10] *CST STUDIO SUITE®Help*, 2020, section: Template Based Post-Processing.
[11] F. Keck, "Project Report 1: Low-Loss Signal Routing on Organic Printed Circuit Boards Through Integration of Waveguide Structures," Rohde and Schwarz, Tech. Rep., 13.02.2020.